Research Article | Vol. 24, No. 22 | 31 Oct 2016 | OPTICS EXPRESS 25684

Optics EXPRESS

# Active switching and tuning of sharp Fano resonances in the mid-infrared spectral region

EUNSONGYI LEE, IN CHEOL SEO, SUNG CHAN LIM, HOON YEUB JEONG, YOUNG CHUL JUN*

*School of Materials Science and Engineering, Ulsan National Institute of Science and Technology (UNIST), Ulsan 44919, South Korea*
**ycjun@unist.ac.kr*

**Abstract:** We propose and analyze a scheme for active switching and spectral tuning of mid-infrared Fano resonances. We consider dielectric resonators made of semiconductor cylinder arrays and block pairs, and theoretically investigate their optical response change due to carrier generation. Owing to sharp optical resonances in these structures and large dielectric constant variations with carrier densities, the significant spectral tuning of Fano resonances is achievable. Furthermore, selective optical pumping in coupled semiconductor structures can even enable dynamic switching of Fano resonances. This leads to a drastic change in the scattering spectra as well as in the near-field intensity. We also observe a stark difference between Fano resonances in cylinder arrays and block pairs. To understand this unusual behavior, we adopt the two coupled oscillator model, and extract the relevant Fano resonance parameters that explain this difference. Our findings and in-depth analyses can be useful for molecular sensors and switching devices in the technologically important mid-infrared spectral region.



**OCIS codes:** (290.0290) Scattering; (050.6624) Subwavelength structures; (230.4555) Coupled resonators; (130.4815) Optical switching devices; (040.3060) Infrared.

## References and links

1. U. Fano, "Effects of configuration interaction on intensities and phase shifts," Phys. Rev. **124**(6), 1866–1878 (1961).
2. Y. S. Joe, A. M. Satanin, and C. S. Kim, "Classical analogy of Fano resonances," Phys. Scr. **74**(2), 259–266 (2006).
3. A. E. Miroshnichenko, S. Flach, and Y. S. Kivshar, "Fano resonances in nanoscale structures," Rev. Mod. Phys. **82**(3), 2257–2298 (2010).
4. B. Luk'yanchuk, N. I. Zheludev, S. A. Maier, N. J. Halas, P. Nordlander, H. Giessen, and C. T. Chong, "The Fano resonance in plasmonic nanostructures and metamaterials," Nat. Mater. **9**(9), 707–715 (2010).
5. W. Park, "Optical interactions in plasmonic nanostructures," Nano Converg. **1**(1), 2 (2014).
6. A. B. Khanikaev, C. Wu, and G. Shvets, "'Fano-resonant metamaterials and their applications," Nanophotonics **2**(4), 247–264 (2013).
7. W. Zhou, D. Zhao, Y.-C. Shuai, H. Yang, S. Chuwongin, A. Chadha, J.-H. Seo, K. X. Wang, V. Liu, Z. Ma, and S. Fan, "Progress in 2D photonic crystal Fano resonance photonics," Prog. Quantum Electron. **38**(1), 1–74 (2014).
8. F. Le, D. W. Brandl, Y. A. Urzhumov, H. Wang, J. Kundu, N. J. Halas, J. Aizpurua, and P. Nordlander, "Metallic nanoparticle arrays: a common substrate for both surface-enhanced Raman scattering and surface-enhanced infrared absorption," ACS Nano **2**(4), 707–718 (2008).
9. A. A. Yanik, A. E. Cetin, M. Huang, A. Artar, S. H. Mousavi, A. Khanikaev, J. H. Connor, G. Shvets, and H. Altug, "Seeing protein monolayers with naked eye through plasmonic Fano resonances," Proc. Natl. Acad. Sci. U.S.A. **108**(29), 11784–11789 (2011).
10. E. Semouchkina, R. Duan, G. Semouchkin, and R. Pandey, "Sensing based on Fano-type resonance response of all-dielectric metamaterials," Sensors (Basel) **15**(4), 9344–9359 (2015).
11. A. E. Miroshnichenko and Y. S. Kivshar, "Fano resonances in all-dielectric oligomers," Nano Lett. **12**(12), 6459–6463 (2012).
12. M. Pu, M. Song, H. Yu, C. Hu, M. Wang, X. Wu, J. Luo, Z. Zhang, and X. Luo, "Fano resonance induced by mode coupling in all-dielectric nanorod array," Appl. Phys. Express **7**(3), 032002 (2014).
13. M. Song, H. Yu, C. Wang, N. Yao, M. Pu, J. Luo, Z. Zhang, and X. Luo, "Sharp Fano resonance induced by a single layer of nanorods with perturbed periodicity," Opt. Express **23**(3), 2895–2903 (2015).

#274829 http://dx.doi.org/10.1364/OE.24.025684
Journal © 2016 Received 30 Aug 2016; revised 6 Oct 2016; accepted 20 Oct 2016; published 26 Oct 2016

Optics EXPRESS


14. J. Zhang, K. F. MacDonald, and N. I. Zheludev, "Near-infrared trapped mode magnetic resonance in an all-dielectric metamaterial," Opt. Express **21**(22), 26721–26728 (2013).
15. F. Zhang, X. C. Huang, Q. Zhao, L. Chen, Y. Wang, Q. Li, X. He, C. Li, and K. Chen, "Fano resonance of an asymmetric dielectric wire pair," Appl. Phys. Lett. **105**(17), 172901 (2014).
16. S. Law, V. Podolskiy, and D. Wasserman, "Towards nano-scale photonics with micro-scale photons: the opportunities and challenges of mid-infrared plasmonics," Nanophotonics **2**(2), 103–130 (2013).
17. R. Stanley, "Plasmonics in the mid-infrared," Nat. Photonics **6**(7), 409–411 (2012).
18. H.-T. Chen, J. F. O'Hara, A. K. Azad, A. J. Taylor, R. D. Averitt, D. B. Shrekenhamer, and W. J. Padilla, "Experimental demonstration of frequency-agile terahertz metamaterials," Nat. Photonics **2**(5), 295–298 (2008).
19. D. J. Cho, W. Wu, E. Ponizovskaya, P. Chaturvedi, A. M. Bratkovsky, S.-Y. Wang, X. Zhang, F. Wang, and Y. R. Shen, "Ultrafast modulation of optical metamaterials," Opt. Express **17**(20), 17652–17657 (2009).
20. P. P. Iyer, N. A. Butakov, and J. A. Schuller, "Reconfigurable semiconductor phased-array metasurfaces," ACS Photonics **2**(8), 1077–1084 (2015).
21. R. Bruck, K. Vynck, P. Lalanne, B. Mills, D. J. Thomson, G. Z. Mashanovich, G. T. Reed, and O. L. Muskens, "All-optical spatial light modulator for reconfigurable silicon photonic circuits," Optica **3**(4), 396–402 (2016).
22. P. Guo, R. D. Schaller, J. B. Ketterson, and R. P. H. Chang, "Ultrafast switching of tunable infrared plasmons in indium tin oxide nanorod arrays with large absolute amplitude," Nat. Photonics **10**(4), 267–273 (2016).
23. C. Kittel, *Introduction to Solid State Physics*, 7th ed. (Wiley, 1995).
24. S. Law, D. C. Adams, A. M. Taylor, and D. Wasserman, "Mid-infrared designer metals," Opt. Express **20**(11), 12155–12165 (2012).
25. M. Cardona, "Electron effective masses of InAs and GaAs as a function of temperature and doping," Phys. Rev. **121**(3), 752–758 (1961).
26. A. Raymond, J. L. Robert, and C. Bernard, "The electron effective mass in heavily doped GaAs," J. Phys. Chem. **12**(12), 2289–2293 (1979).
27. J. S. Blakemore, "Semiconducting and other major properties of gallium arsenide," J. Appl. Phys. **53**(10), R123–R181 (1982).
28. E. S. Koteles and W. R. Datars, "Temperature dependence of the electron effective mass in InSb," Phys. Rev. B **9**(2), 568–571 (1974).
29. E. Litwin-Staszewska, W. Szymańska, and R. Piotrzkowski, "The electron mobility and thermoelectric power in InSb at atmospheric and hydrostatic pressures," Phys. Status Solidi **106**(2), 551–559 (1981).
30. B. R. Bennett, R. A. Soref, and J. A. Del Alamo, "Carrier-induced change in refractive index of InP, GaAs, and InGaAsP," IEEE J. Quantum Electron. **26**(1), 113–122 (1990).
31. M. Nedeljkovic, R. Soref, and G. Z. Mashanovich, "Free-Carrier electrorefraction and electroabsorption modulation predictions for silicon over the 1–14μm infrared wavelength range," IEEE Photonics J. **3**(6), 1171–1180 (2011).
32. Y. C. Jun and I. Brener, "Electrically tunable infrared metamaterials based on depletion-type semiconductor devices," J. Opt. **14**(11), 114013 (2012).
33. V. V. Khardikov, E. O. Iarko, and S. L. Prosvirnin, "A giant red shift and enhancement of the light confinement in a planar array of dielectric bars," J. Opt. **14**(3), 035103 (2012).
34. N. I. Zheludev, S. L. Prosvirnin, N. Papasimakis, and V. A. Fedotov, "Lasing spaser," Nat. Photonics **2**(6), 351–354 (2008).
35. V. A. Fedotov, N. Papasimakis, E. Plum, A. Bitzer, M. Walther, P. Kuo, D. P. Tsai, and N. I. Zheludev, "Spectral collapse in ensembles of metamolecules," Phys. Rev. Lett. **104**(22), 223901 (2010).
36. Y. K. Srivastava, M. Manjappa, L. Cong, W. Cao, I. Al-Naib, W. Zhang, and R. Singh, "Ultrahigh-Q Fano resonances in terahertz metasurfaces: strong influence of metallic conductivity at extremely low asymmetry," Adv. Opt. Mater. **4**(3), 457–463 (2016).
37. B. Gallinet and O. J. F. Martin, "*Ab initio* theory of Fano resonances in plasmonic nanostructures and metamaterials," Phys. Rev. B **83**(23), 235427 (2011).
38. B. Gallinet and O. J. F. Martin, "Influence of electromagnetic interactions on the line shape of plasmonic Fano resonances," ACS Nano **5**(11), 8999–9008 (2011).
39. J. Zhang, W. Liu, Z. Zhu, X. Yuan, and S. Qin, "Strong field enhancement and light-matter interactions with all-dielectric metamaterials based on split bar resonators," Opt. Express **22**(25), 30889–30898 (2014).
40. Y. Moritake, Y. Kanamori, and K. Hane, "Experimental demonstration of sharp Fano resonance in optical metamaterials composed of asymmetric double bars," Opt. Lett. **39**(13), 4057–4060 (2014).
41. V. A. Fedotov, M. Rose, S. L. Prosvirnin, N. Papasimakis, and N. I. Zheludev, "Sharp Trapped-Mode Resonances in Planar Metamaterials with a Broken Structural Symmetry," Phys. Rev. Lett. **99**(14), 147401 (2007).
42. W. Cao, R. Singh, I. A. I. Al-Naib, M. He, A. J. Taylor, and W. Zhang, "Low-loss ultra-high-Q dark mode plasmonic Fano metamaterials," Opt. Lett. **37**(16), 3366–3368 (2012).
43. Y.-W. Huang, H. W. H. Lee, R. Sokhoyan, R. A. Pala, K. Thyagarajan, S. Han, D. P. Tsai, and H. A. Atwater, "Gate-tunable conducting oxide metasurfaces," Nano Lett. **16**(9), 5319–5325 (2016).
44. E. Arbabi, A. Arbabi, S. M. Kamali, Y. Horie, and A. Faraon, "Multiwavelength polarization-insensitive lenses based on dielectric metasurfaces with meta-molecules," Optica **3**(6), 628–633 (2016).

Optics EXPRESS

45. A. Arbabi, Y. Horie, M. Bagheri, and A. Faraon, "Dielectric metasurfaces for complete control of phase and polarization with subwavelength spatial resolution and high transmission," Nat. Nanotechnol. **10**(11), 937–943 (2015).
46. T. P. Steinbusch, H. K. Tyagi, M. C. Schaafsma, G. Georgiou, and J. Gómez Rivas, "Active terahertz beam steering by photo-generated graded index gratings in thin semiconductor films," Opt. Express **22**(22), 26559–26571 (2014).
47. N. Yu, P. Genevet, M. A. Kats, F. Aieta, J. P. Tetienne, F. Capasso, and Z. Gaburro, "Light propagation with phase discontinuities: generalized laws of reflection and refraction," Science **334**(6054), 333–337 (2011).

## 1. Introduction

Fano resonances were initially studied in interacting quantum systems [1]. Their physical origin can be attributed to the interference of a continuum (or broad) state and a discrete (or narrow) state [2, 3]. For example, Fano resonances were observed in the absorption spectra of atomic gases due to the interaction of a continuum of propagating modes with a localized, discrete state. They are often characterized by asymmetric spectral line profiles, instead of typical symmetric line shapes in isolated single resonances. Fano resonances are also accompanied by a drastic change in phase around the resonance frequency.

Optical analogues of Fano resonances have been also studied in various nanostructures [4–7]. These optical Fano resonances can occur due to the optical interaction between broad and narrow modes with different scattering pathways for the incident wave. For example, such Fano resonances were studied in plasmonic nanostructures, consisting of well-designed metallic nanoparticles [8]. Optically broad (bright) and narrow (dark) modes existing in a metal nanoparticle array can interact together, generating asymmetric line shapes in the scattering spectrum. Strong field enhancement in Fano structures can be useful for molecular sensors or other type of optical devices [9, 10]. But, the inherent metal losses and broad scattering spectra of plasmonic Fano structures can severely limit the ultimate performance of optical devices – e.g. the resolution limit for optical sensors.

Very recently, ultra-sharp Fano resonances were studied in dielectric Mie resonators, which do not suffer from metal losses [11–15]. In this case, Mie-type resonances in dielectric nanostructures can provide both broad and narrow modes. For example, a broad dipolar resonance can interact with a higher-order, narrow Mie resonance to induce a Fano resonance. These dielectric Fano structures can exhibit ultra-sharp optical spectra together with strong field enhancement and steep spectral dispersion at the resonance frequencies. These features are highly desirable for high-performance optical sensors and switching devices.

In this paper, we propose a novel scheme for actively tunable Fano resonant structures in the mid-infrared (mid-IR) region. The mid-IR spectral range is technologically important for a number of applications, including chemical sensing and thermal radiation control [16, 17]. Here, we adopt two semiconductor structures as dielectric Fano resonators – cylinder arrays and block pairs –, and theoretically investigate their dynamic control of optical responses. Fano resonances can also occur in dielectric photonic crystal structures [7], but here we focus on simpler Mie resonators.

We show that local carrier generation in coupled semiconductor structures can induce active tuning or switching of Fano resonances in the mid-IR region. Such carrier generation can be achieved with optical pumping above the semiconductor bandgap energy [18–22]. We first show that the carrier density variation in semiconductor cylinder arrays can result in large spectral tuning of sharp Fano resonances. Then, we consider *symmetric* block pairs made of semiconductor materials, which do not exhibit Fano resonances normally. But, with selective optical pumping of one element only, we can effectively create an *asymmetric* block pair with different dielectric constants, and thus induce very sharp Fano resonances. Therefore, we show that dynamic switching of sharp Fano resonances is possible with selective optical pumping in coupled semiconductor structures. This active on/off switching induces a drastic change in the scattering spectra as well as in the near-field intensity and distribution. We find that the maximum electric field intensity can be enhanced more than three orders of magnitude with optical pumping. Due to sharp optical resonances and large

Optics EXPRESS

dielectric constant variations with carrier densities in compound semiconductors, the significant control of Fano resonances is achievable.

We also observe very different Fano resonance behavior in cylinder arrays and block pairs. In cylinder arrays, both resonance sharpness and resonance intensity are reduced with higher doping densities, due to increased ohmic losses in semiconductor. In stark contrast, block pairs exhibit increased resonance intensities while the resonance sharpness still decreases. To understand this unusual behavior, we adopt two coupled oscillator model that provide analytic expressions for Fano resonance line shapes and related parameters. By fitting the reflection spectra obtained from numerical simulations to these analytic equations, we extract the important Fano resonance parameters (e.g. modulation damping parameter *b*) and explain the observed behavior.

Our findings and analyses can find various applications in the technologically important mid-IR region, such as molecular sensors and general wave manipulation devices for thermal radiation.

## 2. Models and methods

The optical response of materials is determined by their dielectric constants. Figure 1 shows the dielectric constant $\varepsilon$ of *n*-doped GaAs and InSb as a function of doping level, which can be calculated from the Drude model [23, 24]:

$$\varepsilon = \varepsilon_\infty \left( 1 - \frac{\omega_p^2}{\omega^2 + i\omega\Gamma} \right) \tag{1a}$$

where

$$\omega_p^2 = \frac{Nq^2}{\varepsilon_0 \varepsilon_\infty m^*} \tag{1b}$$

Here $\varepsilon_\infty$ is the high frequency dielectric constant, $\omega$ is the angular frequency of incident light, $\omega_p$ is the plasma frequency, $N$ is the electron density, $m^*$ is the electron effective mass, and $\Gamma$ is the relaxation frequency. The relevant parameters are obtained from the literature [25–29]. In both cases, the real (solid line) and imaginary (dotted line) parts of dielectric constants are shown. Following Eq. (1), the real part gradually decreases as the doping level increases, while the imaginary part (i.e. optical loss) increases.

Many compound semiconductors have small effective masses and high electron mobilities (therefore low damping rate $\Gamma$). Their optical constants in the IR spectral region are very sensitive to free charge carrier densities, and their imaginary values are relatively small [30, 31]. Therefore, they are highly suitable for actively tunable dielectric Fano resonators. Furthermore, the large dielectric constants of semiconductors make the resonant structures smaller and more compact. The free carrier density $N$ can be modulated optically by pumping the semiconductor with visible-frequency radiation that has higher energy than the semiconductor bandgap: $E_g$(GaAs) = 1.4 eV, $E_g$(InSb) = 0.23 eV at room temperature. Electrical injection or depletion is also potentially usable for dynamic tuning and switching [32]. But, in that case, we need more elaborate device structures for electrical contacts and coupled resonant structures. Therefore, in this work, we have in mind optical pumping for dynamic carrier generation.

InSb has a much smaller electron effective mass ($m_{InSb}^* = 0.014m_0$) than that of *n*-GaAs ($m_{GaAs}^* = 0.067m_0$), where $m_0$ is the free electron mass. Thus, InSb shows a larger variation of dielectric constants with the doping level. So, we can expect that InSb could be a better material for active tuning and switching. In both cases, the imaginary parts are small enough to observe sharp Fano resonances in the considered spectral region. *P*-doped GaAs or InSb have much larger hole effective masses, so their optical constants are not so sensitive as much

Optics EXPRESS

as *n*-doped semiconductors. So, here we consider only *n*-doped semiconductors. Silicon is another common semiconductor material, but it has a much larger electron effective mass ($m_{Si}^* = 0.98m_0$) and thus we do not consider it here, either.

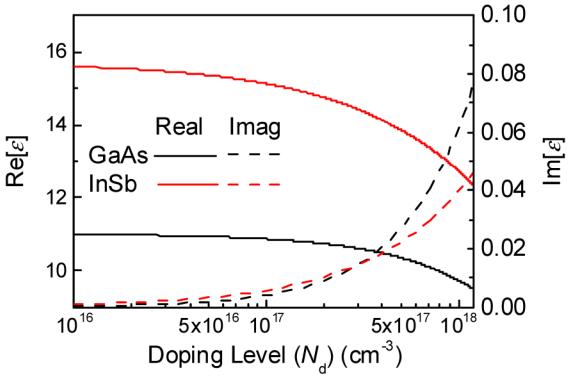


Fig. 1. The dielectric constants $\varepsilon$ of *n*-doped GaAs and InSb at room temperature as a function of doping level at $\lambda = 10$ μm, which are calculated from the Drude model. The relevant Drude parameters are obtained from the literature. The doping level varies from $10^{16}$ $cm^{-3}$ to $10^{18}$ $cm^{-3}$. The solid lines are the real parts of the dielectric constants for GaAs (black) and InSb (red), while the dotted lines are the imaginary parts.

In the next section, we will consider two semiconductor Fano structures: (i) cylinder arrays and (ii) coupled block pairs. We investigate their dynamic control of optical responses with numerical simulations. FDTD (finite difference time domain) and Comsol FEM (finite element method) simulations were used to simulate the reflection spectra and near-field distributions. In these simulations, we employed the dielectric constants given in Fig. 1 to model the optical response for different carrier densities in optically-coupled semiconductor structures. We also present the analytic expressions for Fano resonances based on the two coupled oscillator model, and explain the different behavior in cylinder arrays and block pairs.

## 3. Results and discussion

### *3.1 Cylinder arrays*

We first consider mid-IR Fano resonances in a semiconductor cylinder array. Figure 2(a) shows a schematic of the cylinder array that we are studying here. For simplicity, we consider the cylinder array in free space, which is infinite in the *z* direction. Incident light propagates along the *x*-axis and is polarized along the cylinder axis (i.e. in the *z* direction). Similar Fano resonances can also occur in an array of semiconductor rectangular beams. Although the fabrication of free-standing rectangular beams is more feasible with lithographic pattering and undercut etching, we limit our studies here to cylinder arrays for simplicity. The coupled quadrupolar Mie resonance mode forms a dark mode. The interference of this narrowband mode with a broad Fabry-Perot resonance results in very sharp Fano resonances in the dielectric cylinder array [12, 13]. Figure 2(b) shows the $E_z$ field distribution for the Fano resonance in the InSb cylinder array (cylinder diameter: 2.96 μm, array period: 4 μm), which has the resonance around 10 μm in wavelength. This field profile shows coupled quadrupoles in the cylinder array.

The reflection spectra for InSb cylinder arrays with various periods (*P*: 3.2 μm ~4 μm) are plotted in Fig. 2(c). These spectra clearly show asymmetric line shapes which are characteristic of Fano resonances. The dips in the reflection spectra correspond to dark mode frequencies [6]. We notice that the sharpness of the resonance strongly depends on the array period, which are related to the radiative loss in the dielectric cylinder. In Fig. 2(c), as the

Optics EXPRESS

period increases, the initially broad resonance peak and dip get rapidly sharper. It is interesting to note that the peak of the resonance is almost pinned and only the dip is blue-shifted when the period increases, leading to very sharp resonances. As the array period increases further ($P$ > 4.3 μm), the sharp Fano resonance becomes broader again (not shown here). The accurate Q factors of Fano resonances can be obtained through fitting with Fano lineshapes. But it involves more fitting parameters than Lorentzian lineshapes, and can result in numerical errors. To avoid this issue, we introduce a simpler definition of the resonance sharpness: $\tilde{Q}$ = f/Δf (f: the middle of peak and dip frequencies, Δf: the difference between peak and dip frequencies), which gives good estimation for the resonance sharpness [13, 14, 33]. These are illustrated in Fig. 2(d) as a function of the period. The highest $\tilde{Q}$ of the Fano resonance occurs at a specific period value ($P$ ~4.2 μm), and it drops quickly away from this optimal value. In this cylinder array structure, ultra-sharp Fano resonances ($\tilde{Q}$ > $10^4$) occur at reasonably large gap sizes (> 1 μm). This makes actual fabrication readily feasible with standard lithographic techniques. The drastic change in the resonance sharpness is related to the strong suppression of the radiative loss near the optimal period [34]. This effect has been also called 'spectral collapse' [35], and attributed to the coherent nature of the Fano resonance over the whole cylinder array.

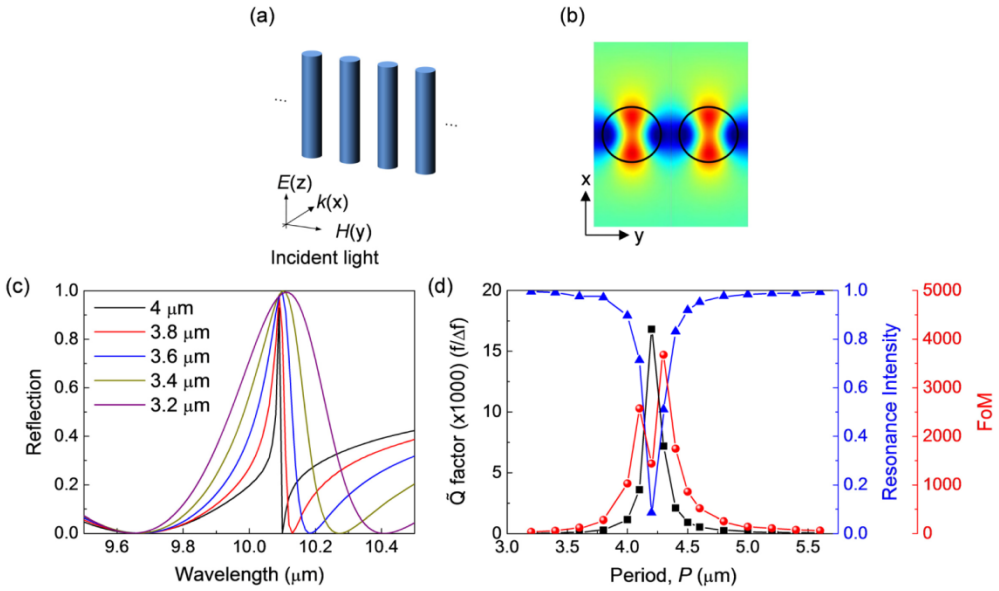


Fig. 2. Fano resonance in a semiconductor cylinder array. (a) Schematic illustration of an infinite cylinder array. (b) The $E_z$ field profile in the InSb cylinder array (diameter: 2.96 μm, period: 4 μm). (c) Reflection spectra for various periods. (d) Resonance sharpness ($\tilde{Q}$), resonance intensity, and FoM as a function of the array period $P$, showing the maximum $\tilde{Q}$ larger than $\tilde{Q}$ ~$10^4$ around $P$ = 4.2 μm.

In fact, near the optimal period (P ~4.2 μm), we find that the intensity of the Fano resonance decreases rapidly, where we define the resonance intensity as the difference between reflection intensities at the peak and dip positions of the asymmetric Fano line (Fig. 2(d)). That is, the resonance intensity shows a rather minimum value when $\tilde{Q}$ becomes the maximum. We can define the figure of merit (FoM) as the product of the resonance sharpness ($\tilde{Q}$) and the resonance intensity [36]. We note that the FoM has maxima a little away from

Optics EXPRESS

the optimal period (P ~4.2 μm), because the resonance intensity has the minimum at those points.

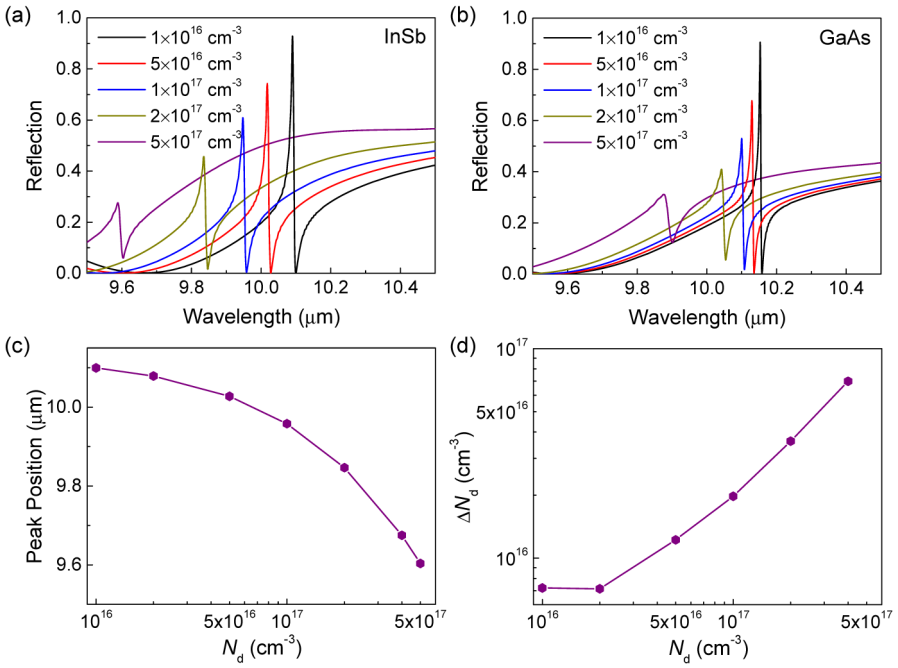


Fig. 3. Spectral tuning of dielectric Fano resonances. The reflection spectra of (a) InSb and (b) GaAs cylinder arrays for different doping levels. We obtain larger spectral tuning for the InSb array due to a larger dielectric constant change, as shown in Fig. 1. (c) Fano resonance peak shift as a function of carrier density of the InSb cylinder array. (d) Carrier density change ($\Delta N_d$) required to tune the resonance by the unit line width, as a function of $N_d$.

Now we consider the effect of carrier densities on Fano resonances in InSb and GaAs cylinder arrays. Figures 3(a) and 3(b) show the reflection spectra for InSb (diameter: 2.96 μm, period: 4 μm) and GaAs (diameter: 3.5 μm, period: 5 μm) cylinder arrays for several different carrier densities $N_d$. The cylinder geometry was chosen to be resonant around 10 μm in both cases. GaAs has a smaller refractive index than InSb, so we adopted slightly larger cylinders to have resonances in the same spectral region. As the carrier density $N_d$ increases, the real part of dielectric constants decrease for both InSb and GaAs (Fig. 1). Therefore, when $N_d$ increases from $1 \times 10^{16}$ cm$^{-3}$ to $5 \times 10^{17}$ cm$^{-3}$, the Fano resonance blue-shifts for both InSb and GaAs array, as shown in Figs. 3(a) and 3(b). As expected in Fig. 1, we find that larger spectral tuning can be obtained in the InSb structure (up to 0.5 μm) due to a larger dielectric constant change. In other words, weaker optical pumping is adequate for InSb to achieve the same amount of spectral tuning. We also investigated similar spectral tuning for different cylinder periods (that have different $\tilde{Q}$ values), but the amount of spectral tuning remained similar.

As shown in Fig. 3(c), the Fano resonance peak in the InSb array blueshifts gradually as the carrier density $N_d$ increases. We also estimated a carrier density change ($\Delta N_d$) required for the unit line width shift of the Fano resonance (Fig. 3(d)). For example, at $N_d = 10^{16}$ cm$^{-3}$, the resonance line width is only 0.016 μm, and $\Delta N_d = 7.21 \times 10^{15}$ cm$^{-3}$ is required to tune the resonance peak by the unit line width. At $N_d = 10^{17}$ cm$^{-3}$, the line width of the Fano resonance becomes broader (0.029 μm), but the required carrier density change still remains very small ($\Delta N_d = 1.974 \times 10^{16}$ cm$^{-3}$).

Optics EXPRESS

As $N_d$ increases, both the resonance sharpness and resonance intensity are reduced due to the increased optical loss (i.e. the imaginary part of dielectric constants, e.g. see the dotted line in Fig. 1), and consequently the FoM decreases. Figure 4(a) shows the three factors that describe the characteristics of Fano resonances.

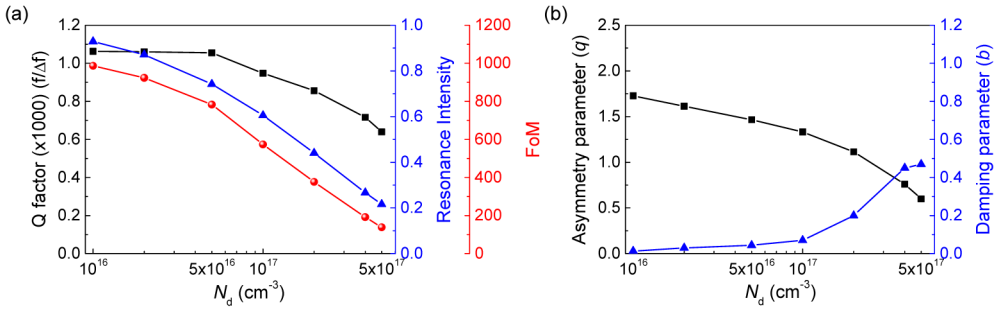


Fig. 4. (a) Resonance sharpness ( $\tilde{Q}$ ), resonance intensity, and FoM (defined as the product of the resonance sharpness and the resonance intensity). Inset is Fano resonance peak shift as a function of $N_d$. (b) Asymmetric paramater, $q$, and damping parameter, $b$, as a function of doping level for InSb cylinder array. All the values in (a) and (b) are extracted from Fig. 3(a).

We also present analytic equations based on the two coupled oscillator model [37]. From this model, we can also obtain the analytic expressions for parameters relevant to Fano resonances that are very useful for understanding Fano resonance behavior. Each oscillator models a bright mode with the resonance frequency $\omega_b$ (having high damping $\gamma_b$) and a dark mode with the resonance frequency $\omega_d$ (having low damping $\gamma_d$). And the two oscillators have a coupling strength $g$. If they are driven by a harmonic external field, the equation of motion can be described as

$$\begin{aligned} \ddot{x}_b + \gamma_b \dot{x}_b + \omega_b^{\,2} x_b + g x_d &= f e^{iwt}. \\ \ddot{x}_d + \gamma_d \dot{x}_d + \omega_d^{\,2} x_d + g x_b &= 0 \end{aligned} \tag{2}$$

where $x_b$ and $x_d$ are the displacements of the oscillators. The amplitude of the highly damped oscillator is given by

$$c_b = \frac{\omega_d^{\,2} + i\gamma_d\omega - \omega^2}{\left(\omega_b^{\,2} + i\gamma_b\omega - \omega^2\right)\left(\omega_d^{\,2} + i\gamma_d\omega - \omega^2\right) - g^2} f. \tag{3}$$

Around $\omega_d$ where the asymmetric line shape arises, assume that $\gamma_d << \gamma_b << \omega_d, \omega_b$, then $\omega_b^{\,2} + i\gamma_b\omega - \omega^2$ is slowly varying in a small frequency region around $\omega_d$, so that it can be considered as a constant. Following Ref [37], we define these parameters; the reduced frequency $\kappa_d = \frac{\left(\omega^2 - \omega_d^{\,2} - \omega_d\Delta\right)}{\Gamma}$, the resonance shift $\Delta = \frac{\left(\omega_d^{\,2} - \omega_b^{\,2}\right)g^2}{|C|^2\,\omega_d}$ and its width $\Gamma = \frac{\gamma_b\omega_d g^2}{|C|^2}$, the asymmetry parameter $q = \frac{\omega_d^{\,2} - \omega_b^{\,2}}{\gamma_b\omega_d}$, and the modulation damping parameter $b = \frac{\gamma_d^{\,2}|C|^4}{\gamma_b^{\,2} g^4}$. Here $C \equiv \omega_b^{\,2} + i\gamma_b\omega - \omega^2$. Then, one can obtain from Eq. (3)

$$\sigma_d = \frac{|c_b|^2}{|A|^2} = \frac{\left(\kappa_d + q\right)^2 + b}{\kappa_d^{\,2} + 1}, \tag{4}$$

Optics EXPRESS

where $|A|^2 = \frac{|f|^2}{|C|^2}$ is the amplitude of the forced oscillator if there is no coupling. Since $\omega_b$ is close to $\omega_d$ (i.e. the bright mode's resonance strength near $\omega_d$ follows a symmetric pseudo-Lorentzian line shape), we can add the following term [38],

$$\sigma_b = \frac{a^2}{\kappa_b^2 + 1}, \tag{5}$$

where $a$ is the maximum amplitude of the resonance, $\kappa_b = \frac{\left(\omega^2 - \omega_b^2\right)}{2W_b\omega_b}$, $W_b$ is the spectral width of the bright mode. A measurable quantity $\sigma_t$ is then represented by the product of two resonances,

$$\sigma_t(\omega) = \sigma_d(\omega)\sigma_b(\omega). \tag{6}$$

The analytic function $\sigma_t$ is used to fit the simulated reflection spectra for the InSb cylinder in Fig. 3(a), and subsequently $q$ and $b$ are extracted as shown in Fig. 4(b) for various $N_d$'s. As $N_d$ increases, the asymmetry parameter $q$ decreases (i.e. the Fano line shape becomes less asymmetric), while the modulation damping parameter $b$ increases (i.e. the Fano resonance intensity is reduced). In this case, the ohmic losses due to increased free carriers are dominant, and both the resonance sharpness and intensity are reduced. However, we will see quite different behavior for the following block pair array.

### 3.2 Coupled block pairs

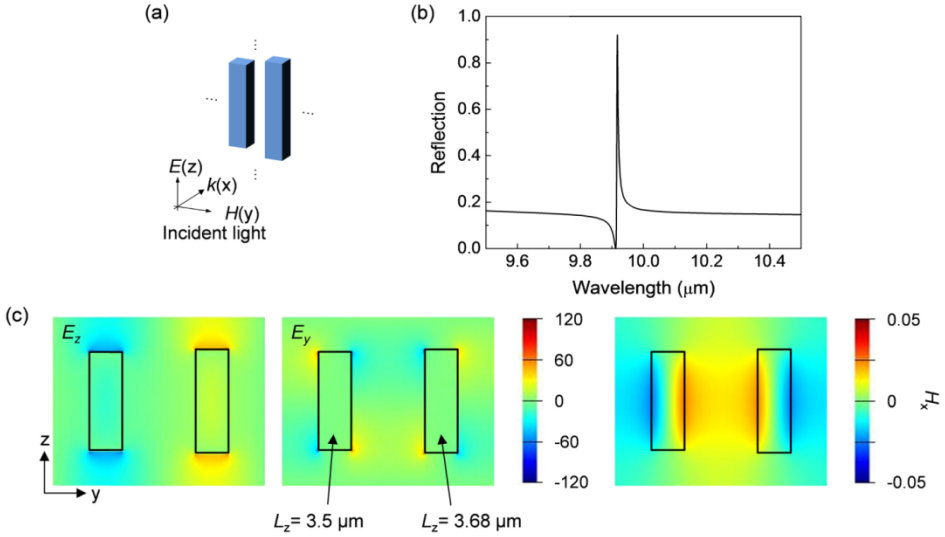


Fig. 5. Dielectric Fano resonance in an asymmetric block pair. (a) Schematic illustration of the geometrically *asymmetric* InSb block pair array (not scaled properly). (b) Reflection spectra showing the Fano resonance for the asymmetric block pair ($L_x$: 1.16 μm, $L_y$: 1.16 μm, period in $y$: 7.6 μm, period in $z$: 6 μm, separation: 1.9 μm), with a size difference of 5% in the $z$ direction. (c) $E_z$ and $E_y$ field profiles of the block pair at the dip of the Fano resonance (left and middle panel, respectively) exhibit an antiparallel induced displacement current. Right panel shows the $H_x$ field, representing the magnetic field normal to the plane.

Now we consider another dielectric structure, which can be used for active switching of Fano resonances. Recently, an asymmetric dielectric particle pair was used to induce very sharp Fano resonances [14, 15, 33, 39]. We first think of a semiconductor block pair, consisting of two closely spaced, parallel bars with slightly different sizes. Specifically, we consider a Fano

Optics EXPRESS

resonance in the geometrically asymmetric InSb block pair located on the *yz* plane. Figure 5 shows the Fano resonance spectrum and field distribution in such asymmetric structure. An incident plane wave is propagating along the *x* axis, as before. The incident light is polarized parallel to the longer side of the block (i.e. *z* axis). The dimension of the block pair was numerically determined to have a resonance around 10 μm. In this structure, symmetry breaking plays an important role. Because phase changes rapidly around the resonance frequency, we can create an anti-parallel displacement current ***D*** in this coupled asymmetric structure. This mode interacts with the incident field very weakly. This dark (narrow) mode interferes with the original broad dipolar resonance in dielectric bars, resulting in a very sharp Fano resonance [14, 15]. For simplicity in numerical simulations, we studied the optical response of such block pair array instead of a single block pair. This allows us to use the periodic boundary condition and simplifies the simulations. The Fano resonance essentially originates from an individual block pair within the unit cell, so we should still obtain similar switching behavior from these array simulations. Again, sharp Fano resonances occur in a purely dielectric structure, which is free of metal losses.

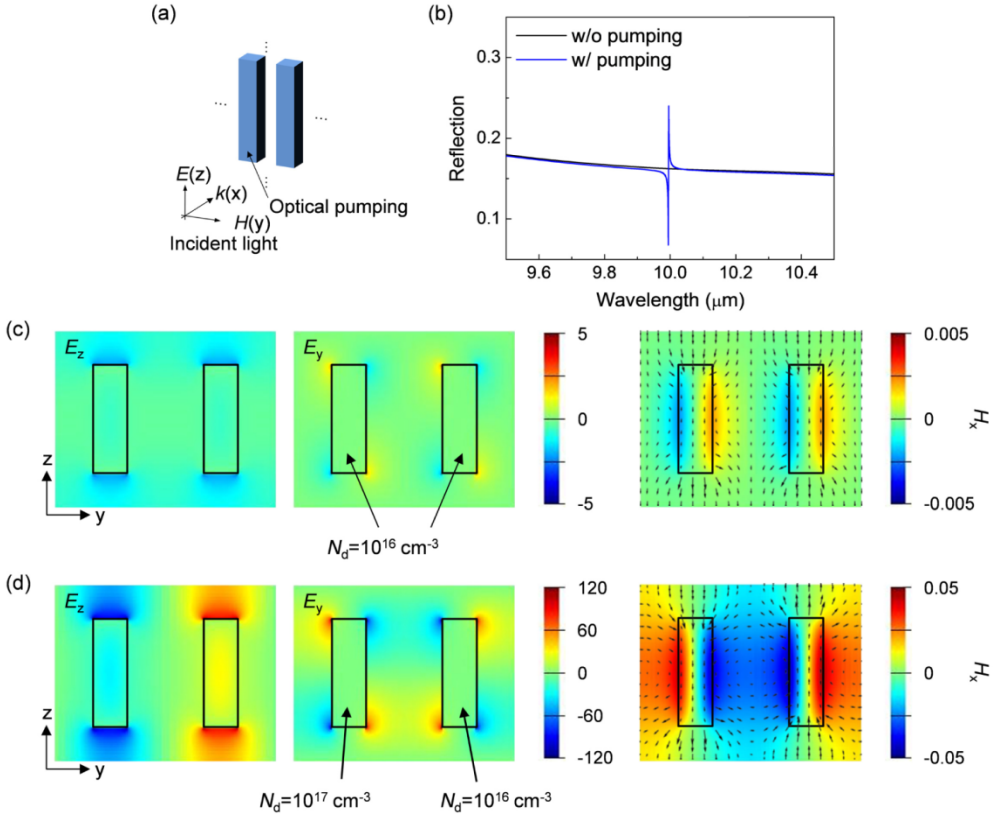


Fig. 6. Active switching of a dielectric Fano resonance. (a) Schematic illustration of the *symmetric* InSb block pair array. (b) Reflection spectra exhibiting a very sharp Fano resonance with selective optical pumping of one block only, compared to that without pumping. Although the physical size is still the same for two blocks, we now have different dielectric constants for them (i.e. they become effectively *asymmetric*). $E_z$, $E_y$, and $H_x$ field profiles of the block pair at the dip of the Fano resonance (left, middle, and right panel, respectively) for (c) without and (d) with selective pumping. Optical pumping induces the strong antiparallel electric field in (d), in contrast to (c) which shows weak, identical electric fields for both blocks. The maximum electric field increases greatly with optical pumping (more than 1000 times enhancement in the *field intensity*). The black arrows in the right panal in (c) and (d) represent the in-plane electric field direction. The length of the arrows is proportional to the electric field intensity.

Optics EXPRESS

Symmetric structures cannot have such dark mode, so they cannot exhibit Fano resonances. Figure 6 illustrates this idea. Here, we show that, with selective optical pumping and carrier generation, we can switch on and off Fano resonances. We start with a symmetric InSb block pair that does not show a Fano resonance. The size of the block pair was slightly modified from the asymmetric one to keep the resonance wavelength around 10 μm. We assume that only the left side block is optically pumped to create more free carriers, and consequently its dielectric constants would be changed. Although the physical size is still the same for two blocks, we now have different dielectric constants for them. So, they have resonances at slightly different wavelengths, and we can again induce the Fano resonance. This idea is manifested clearly in the reflection spectra shown in Fig. 6(b). We assumed that the carrier densities $N_d$ in two InSb blocks are $1 \times 10^{17}$ cm$^{-3}$ (pumped block) and $1 \times 10^{16}$ cm$^{-3}$ (original block). Without optical pumping, the reflection spectrum has a smooth curve without a special resonant feature. But, when we selectively pump a single element only, we have a sharp Fano resonance as we had for the geometrically asymmetric block pair. The Fano resonance is 'switched on' when only one of two blocks is optically pumped. This means that selective optical pumping can induce a unique type of symmetry breaking that can be used for active switching.

To compare these two situations further, we show the electric and magnetic field distributions at the dip of the Fano resonance for the switch-on condition in Fig. 6(d). Figure 6(c) depicts the off condition of the resonance. The $E_z$ field around both blocks in Fig. 6(c) has the same sign and is very weak. Also, the $E_y$ fields for two blocks are identical. On the contrary, Fig. 6(d), corresponding to the switch-on case, exhibits the strong $E_z$ field at the end of the two blocks – more than 40 times stronger in the field magnitude than that without pumping (therefore, more than three orders of magnitude enhancement in the field intensity). The $E_z$ field at the two ends of each block has the same sign, but two blocks show the opposite $E_z$ field, like the asymmetric block pair in Fig. 5(c). It is expected that the induced (displacement) current flow in both blocks are anti-parallel along each bar at the resonant condition [40, 41]. Although selective optical pumping induces differences in the dielectric function of the two blocks, we can see that the magnitude of the electric field around two blocks is still similar to each other. This asymmetric optical pumping can be exploited to achieve ultra-sharp resonances by inducing dark modes with low radiative losses.

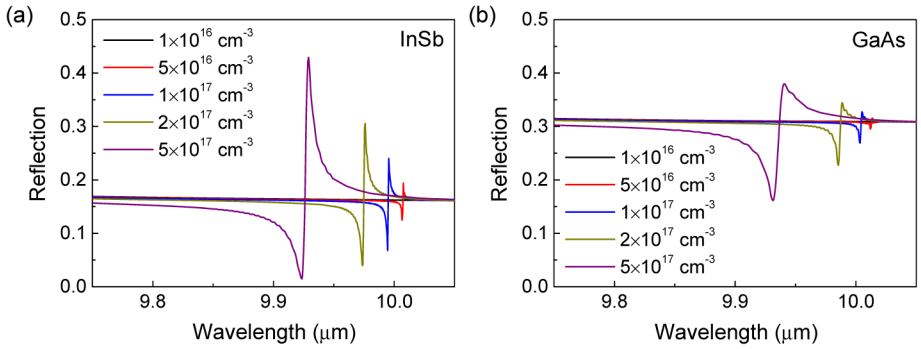


Fig. 7. Active switching of Fano resonances in GaAs and InSb block pairs. Reflection spectra of the block pair for the different doping levels: (a) InSb and (b) GaAs. Free carriers generated by optical pumping can induce a sharp Fano resonance. With increased optical pumping (i.e. increased doping levels), resonance intensities increase in both InSb and GaAs block pairs, while $\tilde{Q}$ decreases.

We further study the effect of carrier densities in InSb and GaAs block pairs. Figure 7 shows the reflection spectra for (a) InSb (size: $1.6 \times 1.6 \times 3.68$ μm$^3$) and (b) GaAs (size: $1.21 \times 1.21 \times 5.26$ μm$^3$) block pair arrays of several different $N_d$'s, which tells the degree of

Optics EXPRESS

*asymmetry* in our structure. (In all cases, the doping levels of the unpumped blocks are kept as $1 \times 10^{16}$ cm$^{-3}$) All geometric sizes are chosen to obtain the sharpest resonance peaks around 10 μm. When the one of two blocks is optically pumped, the Fano resonance is switched on, and sharp peaks appear as shown in Fig. 7. Note that, even for a small difference in $N_d$ (e.g. $5 \times 10^{16}$ cm$^{-3}$), the resonance is switched on (although the resonance intensity is rather small as shown in Fig. 7). Similar to the cylinder array in Fig. 3(a) and (b), when $N_d$ increases, the Fano resonance tend to shift toward shorter wavelengths for larger $N_d$'s, for both InSb and GaAs block pair, due to the reduction in the real part of the dielectric constants as shown in Fig. 1. However, the amount of spectral shift is smaller than that shown in Fig. 3 for both InSb and GaAs block pairs (less than 0.1 μm), when $N_d$ increases from $5 \times 10^{16}$ cm$^{-3}$ to $5 \times 10^{17}$ cm$^{-3}$.

Intriguingly as $N_d$ increases in the considered doping range, the resonance intensity for both InSb and GaAs structures increases, while the resonance slightly gets broader (i.e. $\tilde{Q}$ decreases). This is in stark contrast to Fig. 3(a) and (b), where both resonance intensity and sharpness decrease. Figure 8(a) describes this trend more quantitatively; as $N_d$ increases, the $\tilde{Q}$ decreases but the resonance intensity gradually increases in the considered range of doping densities. Therefore, the FoM for the block pair could have a maximum value at a certain $N_d$ (or at some degree of asymmetry). In fact, we observed a similar trend in Fig. 2(d); $\tilde{Q}$ has the maximum around $P$ ~4.2 μm, while the resonance intensity becomes a minimum at that point. So, the maximum FoM appears somewhat away from the optimal period value ($P$ ~4.2 μm) [36, 42].

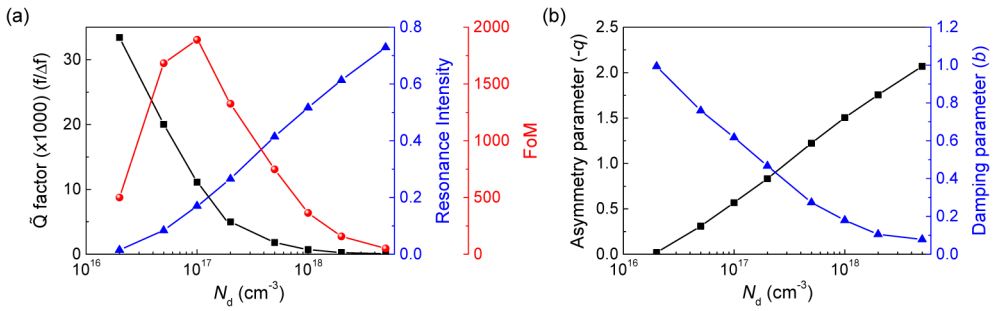


Fig. 8. (a) Resonance sharpness ( $\tilde{Q}$ ), resonance intensity, and FoM (defined as the product of the resonance sharpness and the resonance intensity), (b) Asymmetric parameter $q$, and damping parameter $b$, as a function of the doping level in InSb block pairs. All the values are extracted from Fig. 7(a). With higher optical pumping, the modulation damping parameter $b$ decreases, and the resonance intensity increases.

To understand this behavior more clearly, we again obtained the asymmetry parameter $q$ and the modulation damping parameter $b$ from the simulated spectra. Figure 8(b) shows these parameters, obtained from the reflection spectra of InSb block pairs for various $N_d$'s. (Note that, for the block pair, $q$ has a minus sign, which means that a bright mode is on the left of a dark mode) As $N_d$ increases, $|q|$ increases but $b$ decreases. Note that we had observed the opposite trend for cylinder arrays (Fig. 4(b)). In both cases, optical losses increase as the doping level increases, and $\tilde{Q}$ decreases. However, the modulation damping parameter $b$ is affected by both optical losses and the coupling strength $g$. ($b$ is related to the ratio of the heat energy lost by ohmic losses to the energy that is transferred from a bright mode to a dark mode). In case of coupled block pairs, the effect by the increased coupling strength is more dominant. So, $b$ decreases despite the increased ohmic losses, and the resonance intensity

Optics EXPRESS

increases. Consequently, we observed the increased resonance intensity and the decreased $\tilde{Q}$ value with higher optical pumping.

The mid-IR spectral region corresponds to 3 ~30 μm in wavelength and is technologically important for a number of applications [16, 17]. Many molecules that are important for industrial, environmental, and medical sensing applications have fundamental vibration absorption resonances in the mid-IR region. Different functional groups in molecules have absorption resonances at different wavelengths. Therefore, the absorption spectra can reveal a plenty of chemical information about the molecules and constitute spectral fingerprints for target molecules. Strong field enhancement in resonant Fano structures can increase this vibrational absorption by several orders of magnitude. Furthermore, dielectric Fano structures can exhibit very sharp scattering spectra, together with the strong field enhancement. Therefore, it suits very well for molecular sensing applications. Relatively large gap sizes in the Fano structures that we have studied here make them feasible for reproducible and reliable fabrication. We also expect that dynamic carrier generation could be useful for active beam steering [43–47]. The mid-IR spectral region is also important for thermal imaging and thermal radiation control. Actively tunable and switchable devices in the mid-IR will be very useful for the general manipulation of mid-IR waves, and thus can find useful applications in thermal imaging and thermal radiation control devices.

## 4. Conclusion

In conclusion, we have proposed a novel scheme for active switching and tuning of optical Fano resonances in the technologically important mid-infrared spectral region. We analyzed dielectric Fano structures (semiconductor cylinder arrays and block pairs), and studied their optical response change due to carrier generation. Owing to sharp optical resonances in these structures and large dielectric constant variations with carrier densities in compound semiconductors, significant spectral tuning of Fano resonances is obtainable by optical pumping above the semiconductor bandgap. Furthermore, selective optical pumping and carrier generation in a coupled block pair can even enable dynamic switching of Fano resonances, and thus induce a drastic change in the scattering spectra as well as in the near-field intensity distribution. We find that the maximum electric field intensity can be enhanced more than three orders of magnitude with optical pumping. We also compare Fano resonances in cylinder arrays and block pairs, and find that they exhibit highly different behavior with optical pumping power. With higher optical pumping, cylinder arrays show both reduced resonance sharpness and resonance intensity due to increased optical losses. In contrast, block pairs exhibit increased resonance intensities due to the enhanced coupling between bright and dark modes. We present analytic expressions based on the two coupled oscillator model, and extract the relevant Fano resonance parameters that explain this behavior. These findings and analyses can be very useful for a number of mid-infrared applications, such as molecular sensing and thermal radiation control.

## Funding

NRF grants (No. 2015001948, NRF-2014R1A1A2054108), Research fund (1.150036.01, 1.150114.01, 1.160087.01) of UNIST (Ulsan National Institute of Science and Technology).